The influence of exchange interactions on surface spin waves in a semi-infinite $FeBr_2$ field-induced metamagnet

1994 J. Phys.: Condens. Matter 6 3307

(http://iopscience.iop.org/0953-8984/6/18/007)

J. Phys.: Condens. Matter 6 (1994) 3307–3320. Printed in the UK

The influence of exchange interactions on surface spin waves in a semi-infinite $FeBr_2$ field-induced metamagnet

W Rudziński and W Maciejewski

Institute of Physics, A Mickiewicz University, Ulica Matejki 48/49, PL-60-769 Poznań, Poland

Received 23 January 1993, in final form 25 January 1994

Abstract. Properties of surface spin waves are studied in an $FeBr_2$ field-induced metamagnet that consists of ferromagnetically ordered layers, with intralayer nearest-neighbour ferromagnetic exchange coupling, intralayer next-nearest-neighbour antiferromagnetic exchange coupling and interlayer antiferromagnetic exchange coupling as well as strong three-ion anisotropy. A Green-function method is applied to calculate surface spin-wave modes for the (001) surface and for the paramagnetic phase at low temperatures. By allowing the surface exchange parameters to deviate from the bulk values, the full richness of the surface spin-wave spectra is found. The problem of the stability of the ground state of the system is also discussed.

1. Introduction

In recent years the semi-infinite layered structures of field-induced metamagnets (FIMs) have been the subject of theoretical studies of their surface properties and it has been shown that, in addition to the bulk spin-wave excitations at low temperatures $T \ll T_N$, also surface spin-wave (SSW) modes localized near the surface may occur in both the antiferromagnetic (A) and the paramagnetic (P) phases. The numerical results obtained in [1] for the (001) surface of the $FeBr_2$ and $FeCl_2$ FIM compounds revealed a strong dependence of SSW properties on the crystal structure of these materials. On the assumption of the same exchange interaction and anisotropy on the surface and in the bulk of the sample, the full-zone acoustic-type SSWs were predicted to exist in the A phase, whereas only the optical-type dispersion curves (full-zone SSWs for $FeBr_2$ and truncated SSWs for $FeCl_2$) were found in the P phase.

In [2, 3] the spin-wave characteristics for the above-mentioned FIM crystals were investigated within a more general model where the difference between the effective bulk and surface anisotropy fields were assumed. This enabled the effect of anisotropy on SSWs to be analysed and consequently the modification of the frequency separation between the surface and bulk dispersion curves was obtained. Moreover, by allowing the surface anisotropy parameter to deviate from the bulk value it has been found that, in the P phase, acoustic-type SSW branches lying below the bulk band may also appear in the spectrum.

In this paper we extend the previous studies by investigating the low-temperature properties of SSWs in the semi-infinite FIM crystal with disturbed surface exchange parameters. In order to carry out formal solutions for the SSW and bulk spin-wave characteristics of our FIM system, a generalization of Cottam's [4] Green-function procedure is proposed. For the specific case of the P phase in the $FeBr_2$ structure it will be shown that, when the intralayer exchange parameters describing the coupling of surface spins are allowed to differ from their bulk values, the full range of SSW qualitative features, including new physical solutions, is displayed.

0953-8984/94/183307+14$19.50

Moreover, as a consequence of competition between the surface intralayer and interlayer exchange interactions the problem of the stability of the ground state of the system is under discussion. By constructing the stability diagram we have found different types of critical SSW (below which the surface reconstruction occurs) corresponding to different values of the interlayer exchange parameter. Thus, these diagrams determine the area for experimental and theoretical exploration by imposing limits on the exchange parameters and determining their values sufficient to provide the surface spin stability.

2. General considerations

2.1. The model

The system under study is a semi-infinite FIM filling the half-space $z \geqslant 0$ with ferromagnetically ordered layers parallel to the (001) surface. In the A phase each layer is oriented in a direction opposite to that of the neighbouring layers. If the magnetic field H is applied perpendicular to the surface, then, at a threshold field H_{AP}, a transition occurs to the P phase of high magnetic moment. The system will be represented by the following Hamiltonian, known from [5] as the three-ion model of a FIM:

$$\begin{aligned}\mathcal{H} = -\tfrac{1}{2}\sum_{rr'n} I_{rr'n}(\boldsymbol{S}_{rn}\cdot\boldsymbol{S}_{r'n} + \sigma' S^z_{rn}S^z_{r'n}) + \tfrac{1}{2}\sum_{rn,n-1} J_{rn,n-1}(\boldsymbol{S}_{rn}\cdot\boldsymbol{S}_{rn-1} + \sigma S^z_{rn}S^z_{rn-1}) \\ + \tfrac{1}{2}\sum_{rn,n+1} J_{rn,n+1}(\boldsymbol{S}_{rn}\cdot\boldsymbol{S}_{rn+1} + \sigma S^z_{rn}S^z_{rn+1}) \\ - g\mu_B H\sum_{rn} S^z_n + \mathcal{H}_{rr'n,n-1} + \mathcal{H}_{rr'n,n+1} \qquad (1)\end{aligned}$$

where

$$\mathcal{H}_{rr'n,n-1} = \tfrac{1}{2}\sum_{rr'n,n-1} D_{rr'n,n-1}[S^z_{rn}S^z_{rn-1}(S^z_{r'n})^2 + S^z_{rn}S^z_{rn-1}(S^z_{r'n-1})^2] \qquad (2a)$$

$$\mathcal{H}_{rr'n,n+1} = \tfrac{1}{2}\sum_{rr'n,n+1} D_{rr'n,n+1}[S^z_{rn}S^z_{rn+1}(S^z_{r'n})^2 + S^z_{rn}S^z_{rn+1}(S^z_{r'n+1})^2]. \qquad (2b)$$

Here r denotes the two-dimensional position vector of spins belonging to a given layer labelled by the index n, where $n \geqslant 1$, and $n = 1$ denotes the surface layer. The summations in (1) and (2) always run over different lattice sites. I denotes the ferromagnetic intralayer exchange parameter, whereas J is the antiferromagnetic interlayer parameter.

We assume that the exchange parameters I and J take their bulk values I_b and J_b everywhere except for the surface where they have the values I_s and J_s, respectively. Moreover, note that, in the case of the properties of SSWs in the $FeBr_2$ crystal discussed later, it will be essential to consider the exchange coupling represented by I as a superposition of two competing intralayer interactions: the nearest-neighbour ferromagnetic interaction (I_{s1} and I_{b1} in figure 1) and the next-nearest-neighbour antiferromagnetic interaction (I_{s2} and I_{b2} in figure 1). The coefficients σ and σ' in (1) characterize the uniaxial two-ion anisotropy terms, and H is the applied magnetic field in the z direction. The terms (2) describe the three-ion anisotropic interactions between adjacent layers and for clarity we shall assume henceforth that the anisotropy parameter takes the same value D in the whole sample.

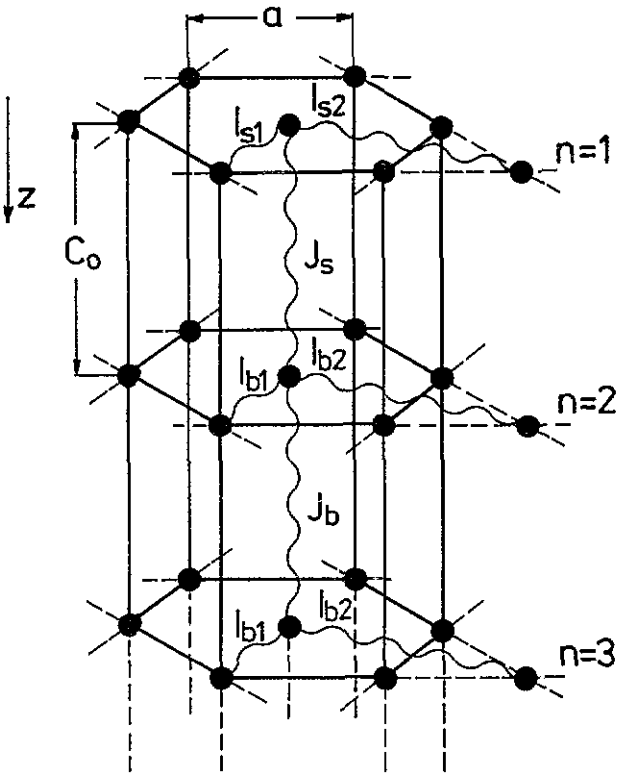

Figure 1. The crystal lattice of the $FeBr_2$ metamagnet with the (001) surface, showing the triangular ordering of Fe^{2+} ions (●) in ferromagnetically ordered layers. The exchange constants between nearest-neighbour and next-nearest-neighbour spins on the surface layer are I_{s1} and I_{s2}, respectively. All other intralayer exchange constants have the bulk value I_b. The exchange constant between spins on the surface and the second layer is J_s. All other interlayer exchange constants have the bulk value J_b. The symbols a and c_0 denote the lattice constant and the layer separation, respectively.

2.2. *Green-function formalism*

The translational symmetry of our semi-infinite metamagnet in individual layers enables us to impose cyclic boundary conditions and to introduce 2D Fourier-transformed Green functions $F_{n,n'}(\boldsymbol{k}_\parallel, \omega)$ defined by

$$F_{n,n'}(\boldsymbol{k}_\parallel, \omega) = \frac{1}{N} \sum_{rr'} G(r, r'; \omega) \exp[-i\boldsymbol{k}_\parallel \cdot (r - r')] \tag{3}$$

where $\boldsymbol{k}_\parallel = (k_x, k_y)$ and $r = (x, y)$ are the two-dimensional wavevector and position vector parallel to the crystal surface, respectively, and N is the number of sites in any layer. The position-dependent Green function at energy ω is $G(r, r'; \omega) = \langle\langle S_r^+; S_{r'}^- \rangle\rangle_\omega$, in standard notation, and it satisfies the equation of motion [6]

$$\omega \langle\langle S_r^+; S_{r'}^- \rangle\rangle_\omega = \frac{1}{2\pi} \langle [S_r^+, S_{r'}^-] \rangle + \langle\langle [S_r^+; \mathcal{H}]; S_{r'}^- \rangle\rangle_\omega. \tag{4}$$

Moreover, we define the following summations for the exchange interactions:

$$p_\gamma(k_\parallel) = \sum_{rn} J_{\gamma rr'n} \exp[ik_\parallel \cdot (r - r')] \qquad (\gamma \equiv \mathrm{s}, \mathrm{b}) \tag{5a}$$

$$v_\gamma(k_\parallel) = \sum_{\xi} J_{\gamma rn,n+1} \exp(ik_\parallel \cdot \xi) \qquad (\gamma \equiv \mathrm{s}, \mathrm{b}) \tag{5b}$$

where ξ in (5*b*) is a vector connecting any site in layer n with its nearest neighbours in layer $n+1$.

In order to carry out the surface mode calculations, explicit analytical expressions for the $F_{n,n'}(k_\parallel, \omega)$-values are required. We have found them from a formal solution of equation (4) at $T \ll T_N$, by extending an approach used previously for semi-infinite ferromagnets [4]. Below we present general results of our calculations for a FIM system in the P phase.

Using (3) together with (4) and evaluating the Green function $\langle\langle [S_r^+; \mathcal{H}]; S_{r'}^- \rangle\rangle_\omega$ on the right-hand side of equation (4) by means of the Tyablikov random-phase approximation as well as the Lines decoupling scheme (for details see [2]) we obtain a set of linear coupled equations for the quantities $F_{n,n'}(k_\parallel, \omega)$. Next we express these equations in a matrix form as

$$(\mathbf{A} + \Delta)\mathbf{f} = \mathbf{b} \tag{6}$$

where $\mathbf{f}$ and $\mathbf{b}$ are infinite-dimensional column matrices with elements given by

$$f_n = F_{n,n'} \tag{7}$$

$$b_n = \frac{\delta_{n,n'}}{\pi |v_b(k_\parallel)|}. \tag{8}$$

Note that these matrix elements are taken for the index $n \geqslant 1$ and for n' fixed. Moreover, $\mathbf{A}$ in (6) denotes a tridiagonal matrix given by

$$\mathbf{A} = \begin{Vmatrix} d & -\tau^{-1} & 0 & 0 & 0 & 0 & \cdot & \cdot & \cdot \\ -\tau & d & -\tau^{-1} & 0 & 0 & 0 & \cdot & \cdot & \cdot \\ 0 & -\tau & d & -\tau^{-1} & 0 & 0 & \cdot & \cdot & \cdot \\ 0 & 0 & -\tau & d & -\tau^{-1} & 0 & \cdot & \cdot & \cdot \\ \cdot & \cdot & \cdot & \cdot & \cdot & \cdot & \cdot & \cdot & \cdot \\ \cdot & \cdot & \cdot & \cdot & \cdot & \cdot & \cdot & \cdot & \cdot \\ \cdot & \cdot & \cdot & \cdot & \cdot & \cdot & \cdot & \cdot & \cdot \end{Vmatrix} \tag{9}$$

with

$$d = \frac{\omega - \eta}{S|v_b(k_\parallel)|} \tag{10}$$

$$\tau = \frac{v_b(-k_\parallel)}{|v_b(k_\parallel)|}. \tag{11}$$

S in (10) is the spin quantum number whereas the quantity η is given by

$$\eta = g\mu_B H + DS^2(2S+1) + (\sigma' + 1)Sp_b(0) - Sp_b(k_\parallel) - 2(\sigma + 1)Sv_b(0). \tag{12}$$

The perturbing effects due to the surface are formally contained in the matrix $\mathbf{\Delta}$:

$$\mathbf{\Delta} = \begin{Vmatrix} \Delta_1 & \Delta_2 & 0 & \cdot & \cdot & \cdot \\ \Delta_3 & \Delta_4 & 0 & \cdot & \cdot & \cdot \\ 0 & 0 & 0 & \cdot & \cdot & \cdot \\ \cdot & \cdot & \cdot & \cdot & \cdot & \cdot \\ \cdot & \cdot & \cdot & \cdot & \cdot & \cdot \\ \cdot & \cdot & \cdot & \cdot & \cdot & \cdot \end{Vmatrix} \tag{13}$$

where the matrix elements Δ_1, Δ_2, Δ_3 and Δ_4 are defined by

$$\Delta_1 = \frac{(\sigma' + 1)[p_b(0) - p_s(0)] - [p_b(k_\parallel) - p_s(k_\parallel)] - (\sigma + 1)[2v_b(0) - v_s(0)]}{|v_b(k_\parallel)|} \tag{14a}$$

$$\Delta_2 = \frac{v_b(k_\parallel) - v_s(k_\parallel)}{|v_b(k_\parallel)|} \tag{14b}$$

$$\Delta_3 = \frac{v_b(-k_\parallel) - v_s(-k_\parallel)}{|v_b(k_\parallel)|} \tag{14c}$$

$$\Delta_4 = \frac{-(\sigma + 1)[v_b(0) - v_s(0)]}{|v_b(k_\parallel)|} \tag{14d}$$

Finally, we obtain the explicit results for the spin Green functions $F_{n,n'}(k_\parallel, \omega)$ as

$$F_{1,1}(k_\parallel, \omega) = \frac{B_{1,1}}{\pi |v_b(k_\parallel)|} + \frac{\tau x(1 + \tau x \Delta_4 - M)}{\pi |v_b(k_\parallel)| M} \tag{15a}$$

$$F_{1,n'}(k_\parallel, \omega) = \frac{B_{1,n'}}{\pi |v_b(k_\parallel)|} + \frac{\tau x^{n'}(1 - \tau \Delta_2 - M)}{\pi |v_b(k_\parallel)| M} \qquad (n' \geqslant 2) \tag{15b}$$

$$F_{n,1}(k_\parallel, \omega) = \frac{B_{n,1}}{\pi |v_b(k_\parallel)|} + \frac{\tau^{2n-1} x^n (1 - \tau \Delta_2 - M)}{\pi |v_b(k_\parallel)| M} \qquad (n \geqslant 2) \tag{15c}$$

$$F_{n,n'}(k_\parallel, \omega) = \frac{B_{n,n'}}{\pi |v_b(k_\parallel)|} + \frac{\tau^{2n-3} x^{n+n'-3} [\tau x \Delta_1 - (\tau^2 x^2 + 1)(M - 1)]}{\pi |v_b(k_\parallel)| M}$$
$$(n \geqslant 2, n' \geqslant 2) \tag{15d}$$

where

$$B_{n,n'} = \begin{cases} \dfrac{\tau(\tau^{2n} x^{n+n'} - x^{n'-n})}{\tau^2 x^2 - x^{-1}} & (n \leqslant n') \\ \dfrac{\tau^{2n-1}(x^{n+n'} - \tau^{-2n'} x^{n-n'})}{\tau^2 x^2 - x^{-1}} & (n > n') \end{cases} \tag{16}$$

$$M = \tau^3 \Delta_4 x^3 + \tau(\tau \Delta_1 \Delta_4 - \tau \Delta_2 \Delta_3 + \tau^2 \Delta_2 + \Delta_3) x^2 + \tau(\Delta_1 + \Delta_4) x + 1 \tag{17}$$

and where the complex parameter x is defined by

$$\tau x + (\tau x)^{-1} = d \qquad |x| \leqslant 1. \tag{18}$$

For later discussion it will be convenient to express the results for the Green functions $F_{n,n'}(k_\parallel, \omega)$ in terms of the generating function $G_{st}(k_\parallel, \omega)$ specified by

$$G_{st}(k_\parallel, \omega) = \sum_{n=1}^{\infty} \sum_{n'=1}^{\infty} s^n t^{n'} F_{n,n'}(k_\parallel, \omega) \tag{19}$$

where s and t are complex parameters sufficiently small in modulus for the double summations to be convergent. Using (15) together with (19) it may be shown that the explicit expression for the generating function is

$$\begin{aligned} G_{st}(k_\parallel, \omega) = {} & \frac{st\tau x}{\pi |v_b(k_\parallel)|(1 - s\tau^2 x)(1 - tx)(1 - st)} \\ & + \frac{st\tau x[(1 + st)(1 - M) + \tau x \Delta_4 + st\tau x(\Delta_1 + x^2\tau^2\Delta_4 + 2x\tau^2\Delta_2)]}{\pi |v_b(k_\parallel)|(1 - s\tau^2 x)(1 - tx)M} \\ & - \frac{st\tau^2 x^2(s\tau^2 + t)(x\Delta_4 + \Delta_2)}{\pi |v_b(k_\parallel)|(1 - s\tau^2 x)(1 - tx)M}. \end{aligned} \tag{20}$$

Now we can deduce the dispersion relations for the corresponding excitations by examining the poles of $G_{st}(k_\parallel, \omega)$. From (20) it can be seen that $G_{st}(k_\parallel, \omega)$ has poles for the x-values satisfying

$$(1 - s\tau^2 x)(1 - tx)M = 0. \tag{21}$$

From [7] it is known that the bulk spin waves correspond to $|x| = 1$ and thus, in our case, the bulk solutions are obtained by considering the factor $1 - s\tau^2 x$ or $1 - tx$ in the denominator of (20). Hence, the solutions for the parameter s or t are deduced by putting

$$x = (s\tau^2)^{-1} = \tau^{-2} \exp(-2ik_z c_0) \tag{22a}$$

or

$$x = t^{-1} = \exp(2ik_z c_0) \tag{22b}$$

into equation (18). The symbol k_z in (22) stands for the third component of the three-dimensional wavevector $k = (k_\parallel, k_z)$, and c_0 denotes the distance between the layers (figure 1).

The remaining poles of the generating function $G_{st}(k_\parallel, \omega)$ come from the equation

$$M = 0. \tag{23}$$

The solutions of (23) are determined by the parameters Δ_1, Δ_2, Δ_3 and Δ_4 and together with the condition $|x| < 1$ they give SSW modes.

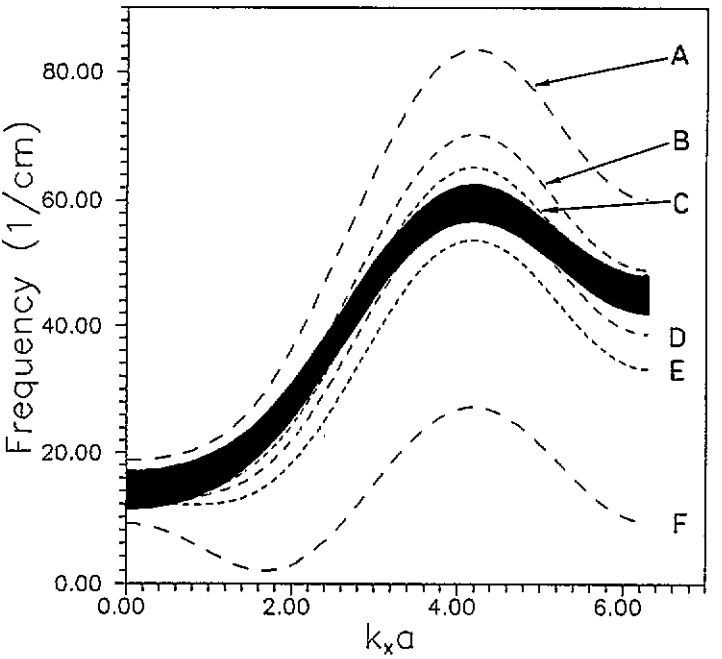

Figure 2. Dispersion relations of SSWs and bulk spin waves in $FeBr_2$ for the P phase, taking $g\mu_B H = 4$ cm^{-1} for the applied field and the parallel vector $k_\parallel$ along the x direction. The shaded area includes the bulk modes. The different SSW curves (- - - -) are as follows all with $I_{s2} = 2$ cm^{-1}: curve A, $I_{s1} = 7.24$ cm^{-1}; curve B, $I_{s1} = 6$ cm^{-1}; curve C, $I_{s1} = 5.5$ cm^{-1}; curve D, $I_{s1} = 5.07$ cm^{-1}; curve E, $I_{s1} = 4.5$ cm^{-1}; curve F, $I_{s1} = 2$ cm^{-1}.

3. Numerical results for $FeBr_2$

Now we shall apply the general formulae introduced in section 2 to calculate the spin-wave characteristics for the specific case of the $FeBr_2$ ($S = 1$) metamagnet. The crystallographic lattice of $FeBr_2$ can be considered as a system of parallel hexagonal layers of iron atoms. The Fe^{2+} ions in one layer are vertically above and below those in adjacent layers (figure 1).

The Fourier transformation of the exchange sum (5*a*) representing the bulk intralayer interaction $p(k_\parallel)$ can be expressed as follows:

$$p_b(k_\parallel) = 2I_{b1}[\cos(k_x a) + 2\cos(k_x a/2)\cos(k_y a\sqrt{3}/2)] + 2I_{b2}[\cos(k_y a\sqrt{3}) + 2\cos(k_y a\sqrt{3}/2)\cos(3k_x a/2)] \tag{24}$$

where I_{b1} and I_{b2} denote nearest-neighbour ferromagnetic and next-nearest-neighbour antiferromagnetic intralayer exchange interaction, respectively, and a stands for the nearest-neighbour distance in the layers (figure 1). A similar formula can be written for surface exchange couplings by substituting I_{b1} and I_{b2} in (24) by I_{s1} and I_{s2}, respectively. The exchange sum (5*b*) is given by

$$v_\gamma(k_\parallel) = J_\gamma \qquad (\gamma \equiv s, b) \tag{25}$$

so that τ in (11) now reads

$$\tau = 1. \tag{26}$$

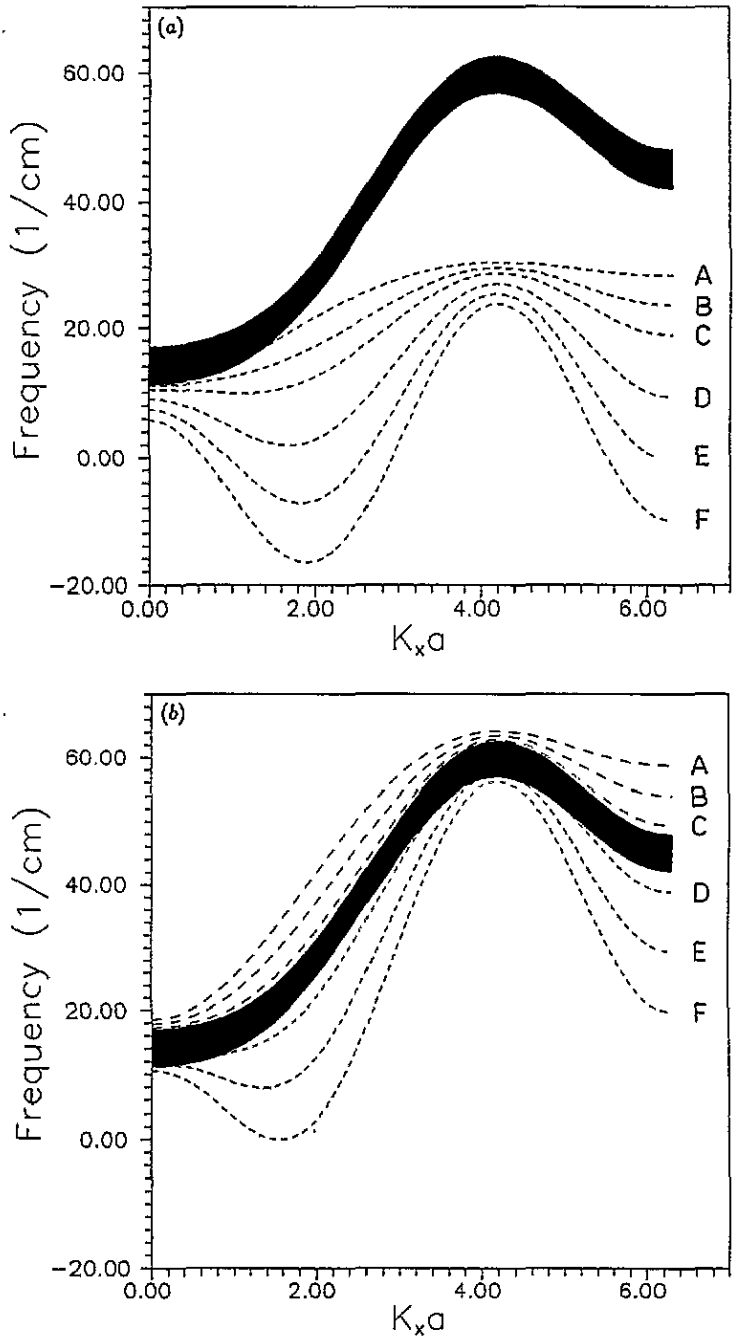
(a)
60.00
40.00
20.00
0.00
-20.00
Frequency (1/cm)
0.00
2.00
4.00
6.00
$K_x a$
A
B
C
D
E
F
(b)
60.00
40.00
20.00
0.00
-20.00
Frequency (1/cm)
0.00
2.00
4.00
6.00
$K_x a$
A
B
C
D
E
F

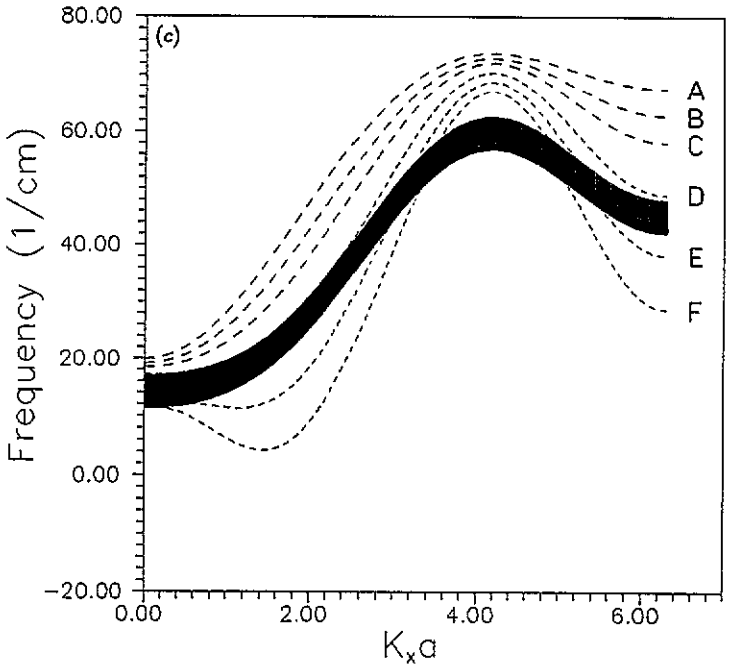

Figure 3. Dispersion relations of SSWs (----) and bulk spin waves (■) in $FeBr_2$ for the P phase, taking $g\mu_B H = 4$ cm^{-1} for the applied field and the parallel vector $k_\parallel$ along the x direction. The different spin-wave curves are as follows: curve A, $I_{s2} = 0$ cm^{-1}; curve B, $I_{s2} = -0.5$ cm^{-1}; curve C, $I_{s2} = -1$ cm^{-1}; curve D, $I_{s2} = -2$ cm^{-1}; curve E, $I_{s2} = -3$ cm^{-1}; curve F, $I_{s2} = -4$ cm^{-1}. The values of the exchange parameter I_{s1} are (*a*) $I_{s1} = 2$ cm^{-1} ($I_{s1} < I_{b1}$), (*b*) $I_{s1} = 5.07$ cm^{-1} ($I_{s1} = I_{b1}$) and (*c*) $I_{s1} = 6$ cm^{-1} ($I_{s1} > I_{b1}$).

The antiferromagnetic exchange interaction $J_{b,s}$ in (25) couples nearest neighbours in two adjacent layers. At this point let us assume that $J_b = J_s = J$ for all layers. This leads to considerable simplification of the general results obtained in section 2 for the spin–spin Green functions, namely

$$\Delta_2 = \Delta_3 = \Delta_4 = 0. \tag{27}$$

Hence, using (17) together with (18), we find the equation for the surface branches $\omega_s(k_\parallel)$ needed in the P phase:

$$\omega_s(k_\parallel) = \eta - SJ(\Delta_1 + 1/\Delta_1). \tag{28}$$

The localization condition $|x| < 1$ for these surface curves reads

$$|\Delta_1| > 1. \tag{29}$$

In a similar manner we calculate the expressions for the bulk spin-wave characteristics by putting (22) into (18):

$$\omega_b(k_\parallel) = \eta + SJ\cos(k_z c_0). \tag{30}$$

To discuss the basic features of the SSWs in $FeBr_2$ we select several representative sets of our results. Numerical calculations were carried out by taking the lattice constants as well

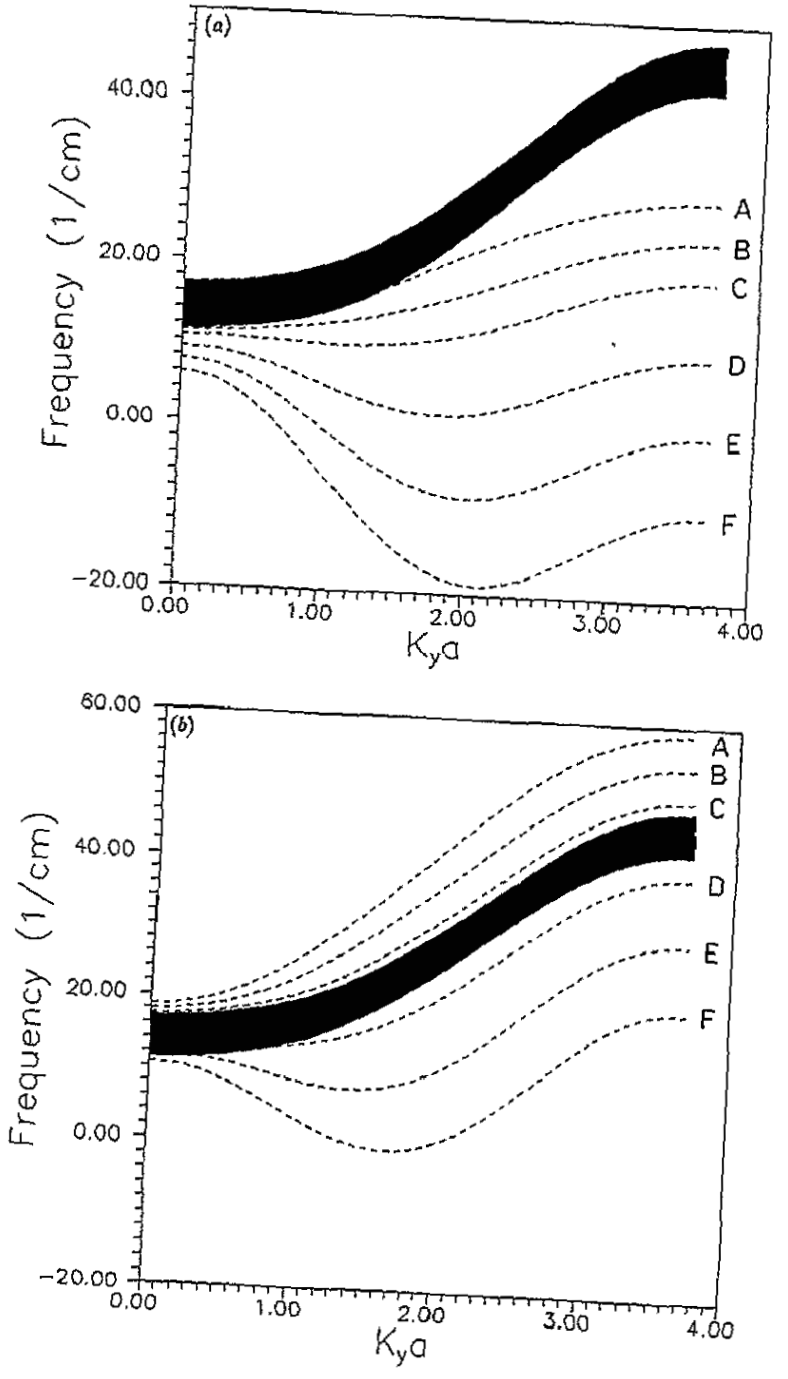
(a)
40.00
20.00
0.00
−20.00
Frequency (1/cm)
A
B
C
D
E
F
0.00
1.00
2.00
3.00
4.00
$K_y a$
(b)
60.00
40.00
20.00
0.00
−20.00
Frequency (1/cm)
A
B
C
D
E
F
0.00
1.00
2.00
3.00
4.00
$K_y a$

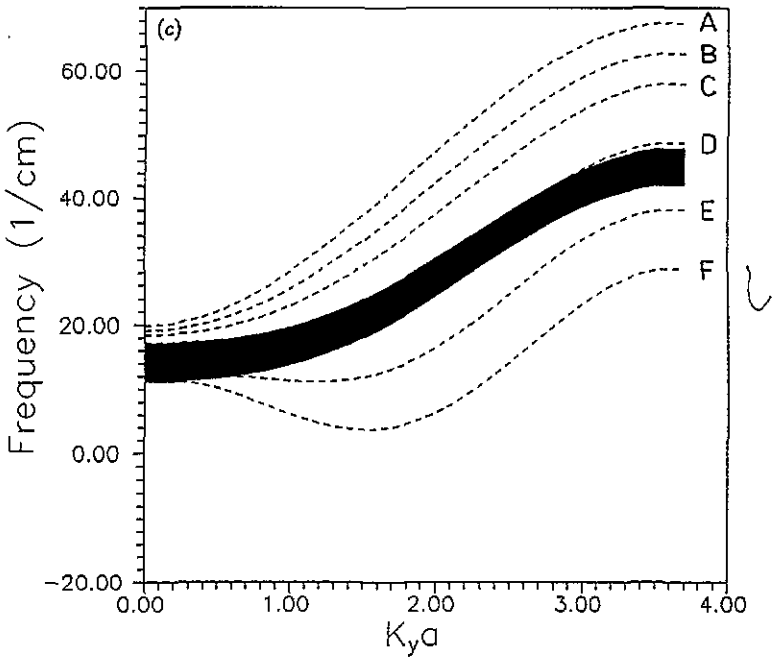

Figure 4. Dispersion relations of SSWs (----) and bulk spin waves (■) in $FeBr_2$ for the P phase, taking $g\mu_B H = 4$ cm^{-1} for the applied field and the parallel vector $k_\parallel$ along the y direction. *The different spin-wave curves are as follows: curve A, $I_{s2} = 0$ cm^{-1}; curve B,* $I_{s2} = -0.5$ cm^{-1}; curve C, $I_{s2} = -1$ cm^{-1}; curve D, $I_{s2} = -2$ cm^{-1}; curve E, $I_{s2} = -3$ cm^{-1}; curve F, $I_{s2} = -4$ cm^{-1}. The values of the exchange parameter I_{s1} are (*a*) $I_{s1} = 2$ cm^{-1} ($I_{s1} < I_{b1}$), (*b*) $I_{s1} = 5.07$ cm^{-1} ($I_{s1} = I_{b1}$) and (c) $I_{s1} = 6$ cm^{-1} ($I_{s1} > I_{b1}$).

as the exchange and anisotropy parameters, according to [8–10], as follows: $c_0 = 1.238$ nm, $a = 0.375$ nm, $I_{b1} = 5.07$ cm^{-1}, $I_{b2} = -1.21$ cm^{-1}, $J = 1.45$ cm^{-1}, $\sigma = \sigma' = 0.28$ and $D = 2.45$ cm^{-1}.

Figure 2 presents the dispersion relations in the applied field $g\mu_B H = 4$ cm^{-1} ($H_{AP} = 3.7$ cm^{-1}) and for the case of the parallel wavevector $k_\parallel$ along the x direction. The shaded area in figure 2 represents the bulk spin-wave modes, whereas the dashed lines A–F represent the surface branches calculated for selected values of I_{s1} and for the case $I_{s2} > I_{b2}$ (the value of I_{s2} is the same for all I_{s1}). Different qualitative features of the SSWs provided by the condition (27) are as follows:

(i) *The full-zone optical SSW* (represented by curve A): the acoustic full-zone SSW branches were predicted to exist for other combinations of I_{s1} and I_{s2} (see figures 5 and 6 later in this section.

(ii) *The truncated SSW* (curve E): these excitations exist only over a limited region of $k_\parallel$ space.

(iii) *The multitruncated SSW* (curves B–D in figure 2): the difference between this case and that represented by curve E is that the surface branches intersect the bulk band more than once and they appear in either the acoustic or the optical regime depending on the competitive relation between intralayer exchange couplings.

(iv) *The soft SSW* (curve F): in this case the ground state of the system becomes unstable and the spin arrangement within the surface of our metamagnet has a symmetry lower than

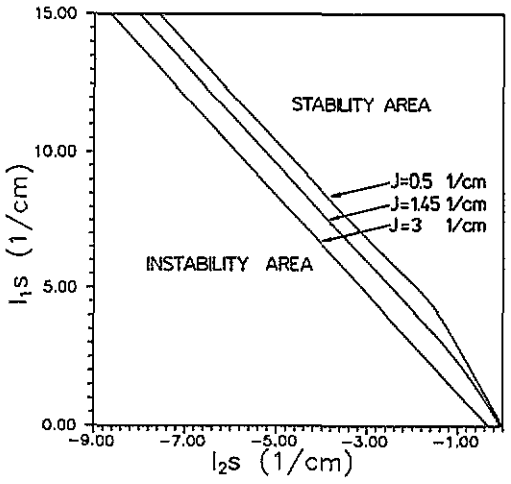

Figure 5. Stability diagrams for the surface region in the (I_{s1}, I_{s2})-plane.

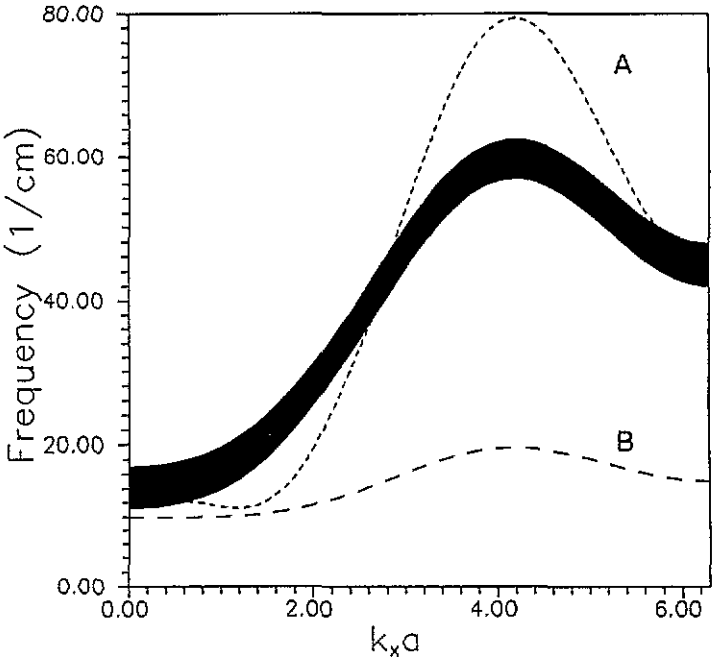

Figure 6. Different types of critical dispersion curve from the stability diagram corresponding to $J = 1.45$ cm^{-1} in figure 5. The surface branch A ($I_{s1} = 7.11$ cm^{-1}; $I_{s2} = -3.63$ cm^{-1}) determines the ground state for $\omega_b[k = (0, 0, \pi)]$, whereas curve B ($I_{s1} = 1.02$ cm^{-1}; $I_{s2} = -0.43$ cm^{-1}) corresponds to the ground-state energy equal to $\omega_s(k_\parallel = 0)$. The shaded area includes the bulk modes.

that in the bulk of the material.

Figures 3 and 4 give a systematic illustration of changes in the above-described SSW properties in the x and y directions, respectively, of the parallel wavevector $k_\parallel$

and for different relations between the values of the exchange parameter I_{s1} and I_{s2}. The consequence of competition between the surface exchange interactions is that, with increasing I_{s1}, the surface modes shift from the acoustic regime (figures 3(*a*) and 4(*a*)) in the direction corresponding to high-energy optical excitations (figures 3(*c*) and 4(*c*)). Simultaneously, we observe qualitative modifications of SSW features, e.g. the soft SSW (curves D in figures 3(*a*) and 4(*a*)) transforms into the truncated and multitruncated SSWs (curves D in figures 3(*b*), 3(*c*), 4(*b*) and 4(*c*)).

Moreover, by varying both I_{s1} and I_{s2} we have constructed diagrams which show regions in the (I_{s1}, I_{s2})-plane where the collinear ferromagnetic arrangement of surface spins is stable, and where it is not. The results of this study are summarized in figures 5 and 6. In figure 5 the critical boundaries dividing the (I_{s1}, I_{s2})-plane into the surface spin-stability and the surface spin-instability area are plotted for different values of the parameter J. We have found that for sufficiently small values of J ($J = 0.5$ and 1.45 cm^{-1} in figure 5) the ground state of the system is determined by the surface frequencies touching both the $\omega_b[k = (0, 0, \pi)]$-values (bottom of the bulk band, curve A in figure 6) and the $\omega_s(k_\parallel = 0)$-values (the full-zone acoustic SSW, curve B in figure 6).

With increasing J the system becomes, as expected, more stable, and simultaneously in diagrams from figure 5 the number of critical points corresponding to the ground-state energy equal to $\omega_b[k = (0, 0, \pi)]$ increases. The stability diagram for $J = 3$ cm^{-1} in figure 5 presents the case when the ground state is determined only by the bottom of the bulk band.

4. Conclusions

This paper provides a theoretical study on the properties of SSWs in the $FeBr_2$ semi-infinite FIM with a (001) surface at low temperatures $T \ll T_N$. The crystal considered reveals the presence of competing intralayer nearest-neighbour ferromagnetic exchange coupling, intralayer next-nearest-neighbour antiferromagnetic exchange coupling and interlayer antiferromagnetic exchange coupling as well as strong three-ion anisotropy. A generalization of the Green-function procedure used previously in [4] for the ferromagnetic case provided us with formal solutions for dispersion relations required to investigate the magnetic properties of the system in the P phase. By allowing the surface exchange interactions to deviate from the bulk values the full range of the SSW spectra has been displayed. We have found that, in addition to the previously evaluated full-zone acoustic and optical SSWs in $FeBr_2$, truncated branches can also exist either above or below the bulk spectrum, depending upon the values of I_{s1} and I_{s2}. An intresting fact is the finding of the multitruncated branches which, to our knowledge, has not been predicted earlier. It is also worth noting that the modification of exchange constants is essential to increasing the frequency separation between SSW and bulk modes. The justification of this becomes evident when we compare the results presented here with those obtained in [1, 3].

On the basis of SSW excitation spectra analysis we have constructed stability diagrams for the gorund state of the system. As a result of a competition between surface intralayer and interlayer exchange interactions the (I_{s1}, I_{s2})-plane is divided by the critical curves into the stability region and the area where the surface reconstruction occurs. We have found that the ground state is determined by the $\omega_s(k_\parallel = 0)$-value or by the bottom of the bulk continuum, $\omega_b[k = (0, 0, \pi)]$. Moreover, from the graphical illustration in the preceding section (figure 5), one can easily see that, the stronger the interlayer parameter J, the more the ground state tends to be determined by the bottom of the bulk band and that simultaneously we observe enlargement of the spin-stability region.

The results obtained in this paper as well as the results of earlier studies [1–3] provide much material for experimental verification, e.g by light-scattering techniques. The critical curves in figure 5 together with different types of dispersion relation indicate the area where one should expect surface spin stability when searching for SSWs lying in the acoustic or optical regime. Moreover, these results allow us to establish the conditions for a sample to provide the splittings of SSWs above or below the bulk modes sufficiently large for experimental detection.

From the viewpoint of the theory, there is a number of possible extensions to this work. We consider it worth reproducing the above analysis for the A phase in $FeBr_2$ as well as for other FIM materials, e.g. $FeCl_2$, of different crystal structures. Also, such problems as the quantitative description of the reconstruction and the calculation of light-scattering intensities are still open to discussion.

References

[1] Baskey J H and Cottam M G 1990 *Phys. Rev.* B **42** 4304
[2] Rudzinski W and Maciejewski W 1992 *Phys. Status Solidi* b **174** 547
[3] Rudzinski W and Maciejewski W 1993 *Phys. Status Solidi* b **175** 247
[4] Cottam M G 1976 *J. Phys. C: Solid State Phys.* **9** 2121
[5] Onyszkiewicz Z and Wierzbicki A 1988 *Physica* B–C **151** 475
[6] Zubarev D N 1960 *Usp. Fiz. Nauk.* **71** 71
[7] Wolfram T and DeWames R E 1972 *Prog. Surf. Sci.* **2** 233
[8] Wyckoff R W 1963 *Crystal Structures* vol 1 (New York: Interscience)
[9] Yelon W B and Vettier C 1975 *J. Phys. C: Solid State Phys.* **8** 2760
[10] Psaltakis G C, Mischler G, Lockwood D J, Cottam M G, Zwick A and Legrand S 1984 *J. Phys. C: Solid State Phys.* **17** 1735